A Flexible Electrode Based on Iron Phosphide Nanotubes for Overall Water Splitting

*Ya Yan, BaoYu Xia, Xiaoming Ge, Zhaolin Liu, Adrian Fisher, Xin Wang **

Prof. X. Wang, Dr Y. Yan, Dr B.Y. Xia

School of Chemical and Biomedical Engineering, Nanyang Technological University, 50 Nanyang Avenue, 639798 Singapore

Prof. Z. Liu, Dr. X. Ge

Institute of Materials Research and Engineering (IMRE), Agency of Science, Technology, and Research (A*STAR), 3 Research Link, Singapore 117602, Singapore

Dr. A. Fisher

Department of Chemical Engineering and Biotechnology, University of Cambridge, New Museums Site, Pembroke Street, Cambridge, CB2 3RA, UK

* Corresponding author. E-mail: WangXin@ntu.edu.sg; Fax: +65 67947553.

Abstract:

Design of cheap and efficient water splitting system for sustainable hydrogen production has attracted increasing attention. We report herein a flexible electrode based on carbon cloth substrate and iron phosphide nanotube coated with an iron oxide/phosphate layer, for overall water splitting. The as-prepared flexible electrode demonstrates remarkable electrocatalytic activity for both H_2 evolution reaction (HER) and O_2 evolution reaction (OER) at modest overpotentials. The surface iron oxide/phosphate formed *in-situ* is proposed to improve the HER activity by facilitating the water dissociation step and serves directly as the catalytically-active component for the OER process.

Molecular hydrogen is a clean and renewable fuel that has the potential to replace fossil fuels in the future. Water splitting, powered by renewable electricity, holds great promise for sustainable hydrogen production,[1] Current devices still rely on the use of noble metal (Pt, Ir, Ru, etc.) -based electrocatalyst and suffer from limited long-term stability.[2] In recent years, tremendous efforts have been devoted to developing low-cost and highly-efficient electrocatalysts.[3] Among them, metal alloys,[4] carbides,[5] sulphides[6] and phosphide[7] based material demonstrate high activity for the hydrogen evolution reaction (HER), while cobalt-phosphate,[8] metal oxides,[9] and hydroxides[10] are found promising for oxygen evolution reaction (OER). While significant progress has been made in this area, there are until now very few earth-abundant catalysts that are capable of catalysing both HER and OER in the same pH range for full water splitting, as almost all the good OER catalysts, work well only in neutral or basic medium, whereas most of the HER catalysts, perform better in acidic medium.[11] Therefore, the current prevailing approaches often result in incompatible integration of the two catalysts and lead to inferior overall performance. To this end, it is crucial to develop Janus catalysts that could work efficiently for both the HER and OER in the same electrolyte. Moreover, the use of a single bifunctional catalyst simplifies the overall system design, lowering the manufacturing cost and thus the cost of the resulting hydrogen.

So far, several Co- or Ni-based bifunctional electrocatalysts have been reported for full alkaline or neutral water splitting.[8b, 12] To expand the scope of the bifunctional materials along with the aim of improving the reaction kinetics at both anode and cathode, we thus turned towards fabrication of Fe-based Janus electrocatalysts because iron-containing phosphide and oxide materials have been showed active for HER or OER.[8a, 13] Here, we show for the first time the construction of the iron phosphide nanotubes (IPNTs) based flexible electrode by reacting the as-prepared iron hydroxide nanotubes with phosphorus vapour. The design demonstrated here open up new possibilities with respect to fabrication of Fe-based Janus catalysts for overall water splitting.

The synthetic strategy for IPNTs electrode is schematically illustrated in **Scheme 1** (for experimental details, see the supporting information). First, aligned and ordered ZnO nanowires (NWs) were grown on carbon cloth (CC) using a wet chemistry method.[14] The obtained ZnO NWs evenly grew on the CC and are about 200-500 nm in diameter and 3-5 um in length (Figure S1a&b).These ZnO NWs were used as the

starting template and immersed in an aqueous solution containing Fe^{3+} at room temperature.[14] The resulting $Fe(OH)_3$ NTs precursors exhibit outer diameters similar to that of ZnO template (200 ~ 500 nm) (Figure S1c&d). Finally, the hydrolysed iron oxide NTs were reacted with phosphorous vapour at 300 ^oC for 30 minutes in a chemical vapour deposition (CVD) apparatus to convert the Fe oxide to the IPNTs.

A representative field-emission scanning electron microscopic (FESEM) image displays the well-defined IPNTs uniformly coated on the CC without damaging its rough nanotube structure (**Figure 1**a). The hollow tube nanostructure is retained after phosphidation, as confirmed by transmission electron microscopy (TEM) technique (Figure 1b). The outer and inner diameters of the IPNTs are ~ 300 and ~100 nm, respectively. The selected-area electron diffraction (SAED) pattern shows concentric rings, composed of bright discrete diffraction spots, indexing to the (111), (202), (211) and (212) planes of orthorhombic FeP (inset of Figure 1b), which are further confirmed by the XRD pattern of the IPNTs (Figure 3a). High resolution (HR)TEM image in Figure 1c reveals the lattice fringe with inter planar distance of 0.19 nm, corresponding to the (211) plane of FeP. A typical scanning (S)TEM image accompanying with energy disperse X-ray (EDX) spectrum demonstrates the existence of elements Fe, P and O (Figure S3 and S4); and the line scanning spectra of Fe, P, O and overall signals across the nanotube further illustrates the nanotube configuration (Figure 1d). Moreover, the presence of O element along the NTs might be due to formation of amorphous iron oxide/phosphate among the top layer of the rough NT (Figure 1c, 1d).

Further investigation into the structure of the IPNTs was obtained from X-ray photoelectron spectroscopy (XPS). The survey spectrum once again confirms the anticipated of Fe, P, O elements in the freshly prepared IPNTs (Figure S5). **Figure 2a-c** give the detailed XPS profiles of Fe 2p, P 2p and O 1s, respectively. In the Fe 2p region (Figure 2a), besides two broad core doublets at 711.8 eV/ 725.5 eV (green line) and 714.1 eV/727.9 eV (blue line), which can be assigned to oxidized state of Fe, such as Fe (III) in iron phosphate and oxides,[15] another set of sharp peaks is observed at lower binding energy relative to the Fe(III), represented by a 707.3 eV ($2p_{3/2}$)/720.0 eV($2p_{1/2}$) doublet, and could be ascribed to FeP, agreeing well with previous reports.[16] The P 2p region (Figure 2b) exhibits two sets of signals. One sharp set with 133.3 eV and 134.1 eV (ratio of 2:1) binding energies correspond to the $2p_{3/2}$ and $2p_{1/2}$ core levels of central phosphorus atoms in phosphate species,[17] while another doublet located at the relatively lower binding energies, corresponding

to $2p_{3/2}$ (129.3 eV) and $2p_{1/2}$ (130.1 eV), could be assigned to low valence of P, FeP in this case.[16b] O1s signal (Figure 2c) is centred at 531.7 eV (O^{2-}) with a peak corresponding to O-P in higher binding energy. As the Fe 2p and O 1s core levels' binding energies of iron oxides are in the same range as those of iron phosphate,[15a] we tentatively describe the surface of the fresh-prepared IPNTs as a combination of iron (III) phosphate and iron oxides species. Moreover, XPS probes only a few nanometres below the surface of the material and indicates a 1:4:11 Fe/P/O ratio, whereas EDX spectroscopy shows a Fe/P/O ratio of 1:0.8:1.7 which probes deeply into IPNTs and reflects bulk composition. Combining XPS and EDX analysis, it is thus concluded that IPNTs is composed of amorphous iron oxide/phosphate component mostly located at the surface and crystalline FeP in the bulk.

The water electrolysis activity of the IPNTs is first confirmed by HER activity through linear sweep voltammetry (LSV) testing in both H_2-saturated 0.5 M H_2SO_4 and 1.0 M KOH electrolytes as shown in **Figure 3** (Figure S6). For comparison, the Pt/C electrode was also measured under the same conditions. As the current collector to construct flexible water splitting electrode, the bare carbon cloth itself is identified to be inactive both in acidic and base electrolytes at potential higher than -0.3 V vs. reversible hydrogen electrode (RHE). In an acidic electrolyte. The onset overpotential (η_{onset}) of the IPNTs was estimated to be ~35 mV and an overpotential (η) of only 88 mV was required to reach a kinetic j_{geo} of -10 mA cm^{-2}. Further scanning towards negative potential produced a dramatic increase in current density (j_{geo}) which even surpassed that of Pt/C at the potential below -144 mV vs. RHE (Figure 3a). In acidic electrolyte, the Pt/C yielded a Tafel slope of 30.4 mV dec^{-1} (Figure 3b), close to the theoretical value of 29.6 mV dec^{-1}, indicating that the process follows the Volmer-Tafel mechanism.[18] The Tafel slope of our IPNTs is 35.5 mV dec^{-1}, which is the highest among all the non-noble metal catalysts reported so far (Table S1) and comparable to that of Pt, indicating that HER kinetics on IPNTs may follow the same mechanism.

Remarkably, in strong alkaline condition (Figure 3c), the η_{onset} of the IPNTs was as low as -31 mV vs. RHE. To reach j_{geo} of 10 mA cm^{-2}, a η of only 120 mV was required. The resulting Tafel plots yielded a Tafel slope of only 59.5 mV dec^{-1}, significantly lower than the value of Pt/C (117.6 mV dec^{-1}) (Figure 3d). It is reported that the Volmer step is the rate-limiting step for HER on Pt/C in alkaline conditions, thus leading to a Tafel slope of about 120 mV dec^{-1}.[11] Therefore the observed Tafel slope of 59.5 mV dec^{-1} here

suggests a Heyrovsky-step-determined Volmer-Heyrovsky mechanism working on the IPNTs catalyst.[18] Beyond the Tafel region, slopes increase as diffusion limitations begin to influence the Tafel kinetics, although the IPNTs exhibited relatively larger onset potentials compared to that of Pt/C, its linear dependence of the logarithmic j_{geo} vs. η (i.e., Tafel region) extends more into higher current density region, suggesting the lower mass transfer resistance at higher current densities, as the 1D directional rough nanotube morphology is beneficial to the timely removal of H_2 bubble from the catalyst surface.[6b, 19] Thus, beyond certain potential, the catalytic current density of the IPNTs surpassed that of Pt/C. Referring to the results above, the HER activity of our IPNTs catalyst is superior to most state-of-the-art HER catalysts (Table S1,), including pure FeP-based HER catalysts.[13a, 20] It could be speculated that the enhanced activity of the IPNTs might be related to the special surface structure and composition of IPNTs, indicating that the nature of the oxide species on the surface is critical.[21] At this point, it is reasonable to propose that iron oxide/phosphate may serve to enhance the water dissociation step as such an effect have been reported for the 3*d* M(Ni, Co, Fe, Mn) hydr(oxy)oxide modified metal catalysts.[22] Thus, with native oxide species present on its surface, IPNTs performs better than the reported FeP catalysts during the alkaline HER process.

Afterwards, steady-state activities of the IPNTs were investigated during 14 h galvanostatic electrolysis at -10 mA cm^{-2} both in acidic and basic electrolyte. As shown in Figure 3e, the IPNTs exhibited superior long-term stability over 14 h in both media. It outperforms other reported FeP-based HER catalysts, especially in alkaline solution.[13a, 20] From the perspective of the electrode design, it is not difficult to understand: the vertical IPNT arrays can improve bubble release from the electrode surface during HER, which thus prevent the hydrogen bubbles from blocking the catalysts during the accumulation process and lead to a better long-term stability. According to the Fe 2p and P 1s spectra along with the atom ratio of Fe/P/O (1:3.4:17 for post-acidic test and 1:1.5:18 for post-basic test), much more oxidized species was detected on the catalyst surface by comparing with the fresh sample, therefore the surface coverage of the catalytic bulk with those iron oxide/phosphate after HER was confirmed (Figure S7). Those formed iron oxide/phosphate film may serve as a protective layer to prevent dissolution of the FeP, and could be one reason for the good stability observed on the IPNTs. By comparing with the Fe/P ratio of 1:4, the deceased P atom could be due to the

dissolution of those free P element that resulted from the special synthesis method. The Faraday efficiency of HER in basic medium was also monitored during a 120 min galvanostatic electrolysis (Figure 3f), showing that the amount of hydrogen evolved corresponded to the theoretical Faraday yield.

We next assessed the catalytic OER activity of IPNTs in O_2-saturated 1.0 M KOH aqueous solution. For comparison, the activity of an IrO_2 catalyst and the bare carbon cloth was measured in parallel. As shown in **Figure 4**a, the anodic current density recorded with the IPNTs catalyst showed a sharp onset of OER current at ~1.48 V vs. RHE (corresponding to a η of 250 mV). To reach the j_{geo} of 10 mA cm^{-2}, a η of only 288 mV was required. The IrO_2 catalyst afforded a similar η_{onset}, but its OER current density fell below that of our IPNTs at ~1.51 V vs. RHE. Although it is hard to point out exactly what kind of oxidized species takes responsibility for the oxygen evolution at this stage, the existence of iron oxide/phosphate, which have been verified to be active species toward OER,[8a, 10b] could act as active sites for the O_2-evolving process. Further analysis of its catalytic kinetics by Tafel plots (Figure 4a inset) resulted in a Tafel slope as low as of 43.0 mV dec^{-1}, that is even better than one of the best commercial OER catalysts, IrO_2 (50.0 mV dec^{-1}). The reduced Tafel slope in the IPNTs implies a more favorable OER kinetics.[23] Considering the low η_{onset}, high j_{geo} and small Tafel slope, the catalytic activity of the IPNTs compares favourably to the most of state-of-the-art OER electrocatalysts (Table S2). Moreover, when biased galvanostatically at 10 mA cm^{-2} on the IPNTs electrodes, the catalyst showed a nearly constant overpotential with merely 13 mV increase during 14 h of continuous operation, whereas the IrO_2 catalyst showed an increase in overpotential by ~60 mV (Figure 4b). Its Faradaic efficiency for the OER was also conducted at constant applied potential for 120 min, suggesting near 100% Faradaic efficiency (Figure S8). To further verify the catalytic role of the surface iron oxide/phosphide for effective OER, XPS profiles of the Fe 2p and P 1s was recorded from the catalyst after the stability test, we found a shift of the Fe 2p peak to the higher binding energy and large oxidized species accumulation (O/P atom ratio 37.5:1) in the tested sample (Figure S9), indicating the increased oxidation states of the surface Fe metal centres. A previous study regarding the design principle for OER catalysts established that materials with high OER activity shall be the ones with high covalence of transition metal-oxygen bonds,[24] which has been successfully used to guide the design of various transition metal OER catalysts. [8a, 25] We believe this is also insightful in explaining the high OER activity of the IPNTs due to the

existence of high valence Fe metal centres on the material surface. Additionally, amorphous Fe_2O_3 and $FePO_4$ supported CC electrodes were also prepared separately (see SI, Figure S10) and their OER activity were examined (Figure S11). It can be seen that both electrodes show much lower performance than the IPNTs and Fe_2O_3 slightly outperforms $FePO_4$. It seems there is some synergistic effect among Fe_2O_3, $FePO_4$ and underneath FeP that render the high OER activity of IPNTs.

Featured with mixed structure of FeP bulk and Fe oxide/phosphate shell, the IPNTs showed an efficient bifunctional catalytic activity for both HER and OER as evidenced by the cyclic voltammetry curve in Figure 4c, a catalytic model illustrating the Janus catalytic mechanism of the material was proposed (Figure 4c inset). Finally, a practical investigation on the Janus performance of IPNTs for overall water electrolysis is demonstrated in a two-electrode configuration (Figure 4d and Figure S12). It showed a current density of 10 mA cm^{-2} at about 1.69 V vs. RHE, representing a combined overpotential of only about 460 mV for HER and OER. Importantly, the potential was stable at this value during a 14 h galvanostatic electrolysis process (Figure 4d inset, Movie S1). We thus believe that the material reported here enjoys bifunctional and synergetic effect with the FeP bulk and iron oxide/phosphate surface, catalytically competent for H_2 and O_2 evolution. The surface iron oxide/phosphate formed *in-situ* not only improve the HER catalytic activity by enhancing the water dissociation step,[22a] but also serves as the catalytically-active component for the OER process.

In summary, a flexible electrode based on iron phosphide nanotubes is successfully prepared for overall water splitting. This material consists of FeP coated with an iron oxide/phosphate layer and mediates H_2 evolution from both acidic and basic aqueous media at modest overpotentials. Remarkably, the surface iron oxide/phosphate formed in situ can be directivity used to catalyse O_2 evolution. Therefore, the flexible IPNTs electrode demonstrates remarkable activity and stability for the overall alkaline electrolyser. These findings in our work open up new possibilities with respect to the fabrication of efficient Janus catalysts with low cost for overall water splitting.

Supporting Information

Supporting Information is available from the Wiley Online Library or from the author.

Acknowledgements

This project is funded by the National Research Foundation (NRF), Prime Minister's Office, Singapore under its Campus for Research Excellence and Technological Enterprise (CREATE) programme. We also acknowledge financial support from the academic research fund AcRF tier 1 (M4011253 RG 7/14) and tier 2 (M4020246, ARC10/15), Ministry of Education, Singapore.

References

[1] a) A. B. Laursen, S. Kegnaes, S. Dahl, I. Chorkendorff, *Energy Environ. Sci.* **2012**, *5*, 5577; b) C. Grimes, O. Varghese, S. Ranjan, in *Light, Water, Hydrogen*, Springer US, **2008**, pp. 35; c) S. Chen, J. Duan, M. Jaroniec, S.-Z. Qiao, *Adv. Mater.* **2014**, *26*, 2925.

[2] T. R. Cook, D. K. Dogutan, S. Y. Reece, Y. Surendranath, T. S. Teets, D. G. Nocera, *Chem. Rev.* **2010**, *110*, 6474.

[3] a) X. Zou, Y. Zhang, *Chem. Soc. Rev.* **2015**, *44*, 5148; b) C. C. L. McCrory, S. Jung, J. C. Peters, T. F. Jaramillo, *J. Am. Chem. Soc.* **2013**, *135*, 16977; c) Y. Zheng, Y. Jiao, M. Jaroniec, S. Z. Qiao, *Angew. Chem. Int. Ed.* **2015**, *54*, 52; d) J. Duan, S. Chen, M. Jaroniec, S. Z. Qiao, *ACS Nano* **2015**, *9*, 931; e) Y. Zheng, Y. Jiao, Y. Zhu, L. H. Li, Y. Han, Y. Chen, A. Du, M. Jaroniec, S. Z. Qiao, *Nat. Commun.* **2014**, *5*, 3783; f) T. Y. Ma, S. Dai, M. Jaroniec, S. Z. Qiao, *Angew. Chem. Int. Ed.* **2014**, *53*, 7281.

[4] Q. Lu, G. S. Hutchings, W. Yu, Y. Zhou, R. V. Forest, R. Tao, J. Rosen, B. T. Yonemoto, Z. Cao, H. Zheng, J. Q. Xiao, F. Jiao, J. G. Chen, *Nat. Commun.* **2015**, *6*, 6567.

[5] a) W. F. Chen, J. T. Muckerman, E. Fujita, *Chem. Commun.* **2013**, *49*, 8896; b) Y. Yan, L. Zhang, X. Qi, H. Song, J. Y. Wang, H. Zhang, X. Wang, *Small* **2012**, *8*, 3350.

[6] a) Y. Yan, B. Xia, Z. Xu, X. Wang, *ACS Catal.* **2014**, *4*, 1693; b) M. S. Faber, R. Dziedzic, M. A. Lukowski, N. S. Kaiser, Q. Ding, S. Jin, *J. Am. Chem. Soc.* **2014**, *136*, 10053; c) Z. Lu, W. Zhu, X. Yu, H. Zhang, Y. Li, X. Sun, X. Wang, H. Wang, J. Wang, J. Luo, X. Lei, L. Jiang, *Adv. Mater.* **2014**, *26*, 2683; d) J. Duan, S. Chen, B. A. Chambers, G. G. Andersson, S. Z. Qiao, *Adv. Mater.* **2015**, *27*, 4234; e) Y. Yan, B. Y. Xia, X. M. Ge, Z. L. Liu, J. Y. Wang, X. Wang, *Acs Appl Mater Inter* **2013**, *5*, 12794; f) Y. Yan, B. Xia, X. Qi, H. Wang, R. Xu, J.-Y. Wang, H. Zhang, X. Wang, *Chem. Commun.* **2013**, *49*, 4884; g) Y. Yan, B. Xia, N. Li, Z. Xu, A. Fisher, X. Wang, *J. Mater. Chem. A* **2015**, *3*, 131.

[7] a) Y. Yan, L. Thia, B. Y. Xia, X. Ge, Z. Liu, A. Fisher, X. Wang, *Adv. Sci.* **2015**, doi: 10.1002/advs.201500120; b) Z. Huang, Z. Chen, Z. Chen, C. Lv, H. Meng, C. Zhang, *ACS Nano* **2014**, *8*, 8121; c) Z. Pu, Q. Liu, P. Jiang, A. M. Asiri, A. Y. Obaid, X. Sun, *Chem. Mater.* **2014**, *26*, 4326.

[8] a) Y. Liu, H. Wang, D. Lin, C. Liu, P.-C. Hsu, W. Liu, W. Chen, Y. Cui, *Energy Environ. Sci.* **2015**, doi: 10.1039/C5EE01290B; b) N. Jiang, B. You, M. Sheng, Y. Sun, *Angew. Chem. Int. Ed.* **2015**, *54*, 6251; c) T. Y. Ma, J. Ran, S. Dai, M. Jaroniec, S. Z. Qiao, *Angew. Chem. Int. Ed.* **2015**, *54*, 4646.

[9] a) S. Du, Z. Ren, J. Zhang, J. Wu, W. Xi, J. Zhu, H. Fu, *Chem. Commun.* **2015**, *51*, 8066; b) Y. Yang, H. Fei, G. Ruan, C. Xiang, J. M. Tour, *ACS Nano* **2014**, *8*, 9518; c) T. Y. Ma, S. Dai, M. Jaroniec, S. Z. Qiao, *J. Am. Chem. Soc.* **2014**, *136*, 13925; d) K. Fominykh, P. Chernev, I. Zaharieva, J. Sicklinger, G. Stefanic, M. Döblinger, A. Müller, A. Pokharel, S. Böcklein, C. Scheu, T. Bein, D. Fattakhova-Rohlfing, *ACS Nano* **2015**, *9*, 5180; e) J. Liang, R. F. Zhou, X. M. Chen, Y. H. Tang, S. Z. Qiao, *Adv. Mater.* **2014**, *26*, 6074.

[10] a) M. Gong, Y. Li, H. Wang, Y. Liang, J. Z. Wu, J. Zhou, J. Wang, T. Regier, F. Wei, H. Dai, *J. Am. Chem. Soc.* **2013**, *135*, 8452; b) W. D. Chemelewski, H.-C. Lee, J.-F. Lin, A. J. Bard, C. B. Mullins, *J. Am. Chem. Soc.* **2014**, *136*, 2843; c) M. S. Burke, M. G. Kast, L. Trotochaud, A. M. Smith, S. W. Boettcher, *J. Am. Chem. Soc.* **2015**, *137*, 3638; d) J. Nai, H. Yin, T. You, L. Zheng, J. Zhang, P. Wang, Z. Jin, Y. Tian, J. Liu, Z. Tang, L. Guo, *Adv. Energy Mater.* **2015**, *5*, doi: 10.1002/aenm.201401880; e) H.-Y. Wang, Y.-Y. Hsu, R. Chen, T.-S. Chan, H. M. Chen, B. Liu, *Adv. Energy Mater.* **2015**, *5*, doi: 10.1002/aenm.201500091; f) W. Ma, R. Ma, C. Wang, J. Liang, X. Liu, K. Zhou, T. Sasaki, *ACS Nano* **2015**, *9*, 1977; g) F. Song, X. Hu, *Nat. Commun.* **2014**, *5*, 4477.

[11] J. Durst, A. Siebel, C. Simon, F. Hasche, J. Herranz, H. A. Gasteiger, *Energy Environ. Sci.* **2014**, *7*, 2255.

[12] a) Z. Peng, D. S. Jia, A. M. Al-Enizi, A. A. Elzatahry, G. F. Zheng, *Adv. Energy Mater.* **2015**, *5*, doi: 10.1002/Aenm.201402031; b) S. Cobo, J. Heidkamp, P. A. Jacques, J. Fize, V. Fourmond, L. Guetaz, B. Jousselme, V. Ivanova, H. Dau, S. Palacin, M. Fontecave, V. Artero, *Nat. Mater.* **2012**, *11*, 802; c) Y. Yang, H. Fei, G. Ruan, J. M. Tour, *Adv. Mater.* **2015**, *27*, 3175; d) L.-A. Stern, L. Feng, F. Song, X. Hu, *Energy Environ. Sci.* **2015**, doi: 10.1039/C5EE01155H; e) M. Ledendecker, S. Krick Calderón, C. Papp, H.-P. Steinrück, M. Antonietti, M. Shalom, *Angew. Chem. Int. Ed.* **2015**, doi: 10.1002/anie.201502438.

[13] a) P. Jiang, Q. Liu, Y. Liang, J. Tian, A. M. Asiri, X. Sun, *Angew. Chem. Int. Ed.* **2014**, *53*, 12855; b) J. F. Callejas, J. M. McEnaney, C. G. Read, J. C. Crompton, A. J. Biacchi, E. J. Popczun, T. R. Gordon, N. S. Lewis, R. E. Schaak, *ACS Nano* **2014**, *8*, 11101; c) H. Wang, H. W. Lee, Y. Deng, Z. Lu, P. C. Hsu, Y. Liu,

D. Lin, Y. Cui, *Nat. Commun.* **2015**, *6*, 7261; d) A. Mendoza-Garcia, H. Zhu, Y. Yu, Q. Li, L. Zhou, D. Su, M. J. Kramer, S. Sun, *Angew. Chem. Int. Ed.* **2015**, doi: 10.1002/anie.201503386.

[14] J. Liu, Y. Li, H. Fan, Z. Zhu, J. Jiang, R. Ding, Y. Hu, X. Huang, *Chem. Mater.* **2010**, *22*, 212.

[15] a) A. P. Grosvenor, B. A. Kobe, M. C. Biesinger, N. S. McIntyre, *Surf. Interface Anal.* **2004**, *36*, 1564; b) B. Lee, C. Kim, Y. Park, T.-G. Kim, B. Park, *Electrochem. Solid-State Lett.* **2006**, *9*, E27.

[16] a) C. Qian, F. Kim, L. Ma, F. Tsui, P. Yang, J. Liu, *J. Am. Chem. Soc.* **2004**, *126*, 1195; b) A. P. Grosvenor, S. D. Wik, R. G. Cavell, A. Mar, *Inorg. Chem.* **2005**, *44*, 8988.

[17] D. Yu, C. Wu, Y. Kong, N. Xue, X. Guo, W. Ding, *J. Phys. Chem. C* **2007**, *111*, 14394.

[18] J. O. M. Bockris, E. C. Potter, *J. Electrochem. Soc.* **1952**, *99*, 169.

[19] Z. Y. Lu, Y. J. Li, X. D. Lei, J. F. Liu, X. M. Sun, *Mater. Horiz.* **2015**, *2*, 294.

[20] Y. Liang, Q. Liu, A. M. Asiri, X. Sun, Y. Luo, *ACS Catal.* **2014**, *4*, 4065.

[21] N. Danilovic, R. Subbaraman, D. Strmcnik, K. C. Chang, A. P. Paulikas, V. R. Stamenkovic, N. M. Markovic, *Angew. Chem. Int. Ed.* **2012**, *51*, 12495.

[22] a) R. Subbaraman, D. Tripkovic, K.-C. Chang, D. Strmcnik, A. P. Paulikas, P. Hirunsit, M. Chan, J. Greeley, V. Stamenkovic, N. M. Markovic, *Nat. Mater.* **2012**, *11*, 550; b) R. Subbaraman, D. Tripkovic, D. Strmcnik, K.-C. Chang, M. Uchimura, A. P. Paulikas, V. Stamenkovic, N. M. Markovic, *Science* **2011**, *334*, 1256.

[23] a) D. K. Bediako, Y. Surendranath, D. G. Nocera, *J. Am. Chem. Soc.* **2013**, *135*, 3662; b) S. Gottesfeld, S. Srinivasan, *J. Electroanal. Chem. Interfacial Electrochem.* **1978**, *86*, 89.

[24] J. Suntivich, K. J. May, H. A. Gasteiger, J. B. Goodenough, Y. Shao-Horn, *Science* **2011**, *334*, 1383.

[25] L. Kuai, J. Geng, C. Chen, E. Kan, Y. Liu, Q. Wang, B. Geng, *Angew. Chem. Int. Ed.* **2014**, *53*, 7547.

Figures and Captions

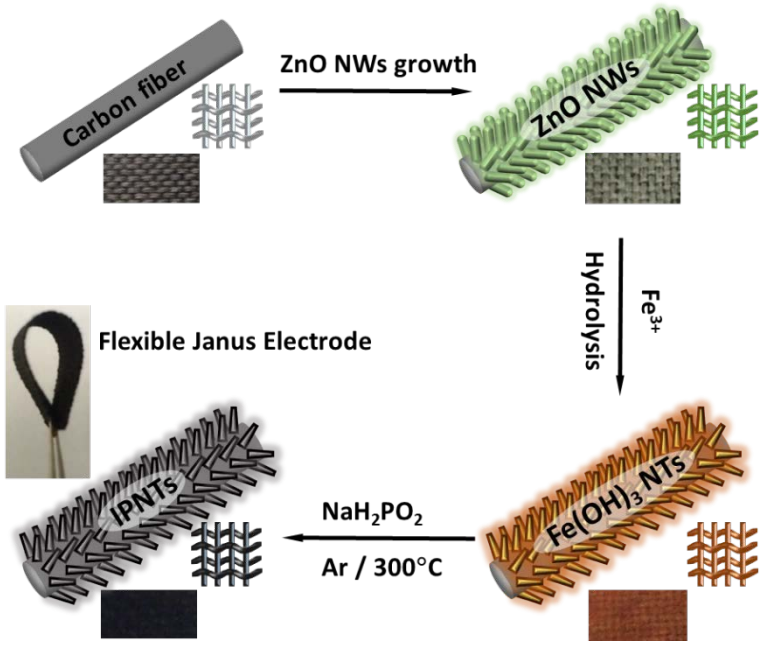

Scheme 1. Schematic diagram illustrating the synthesis procedure of IPNTs based flexible bifunctional electrode.

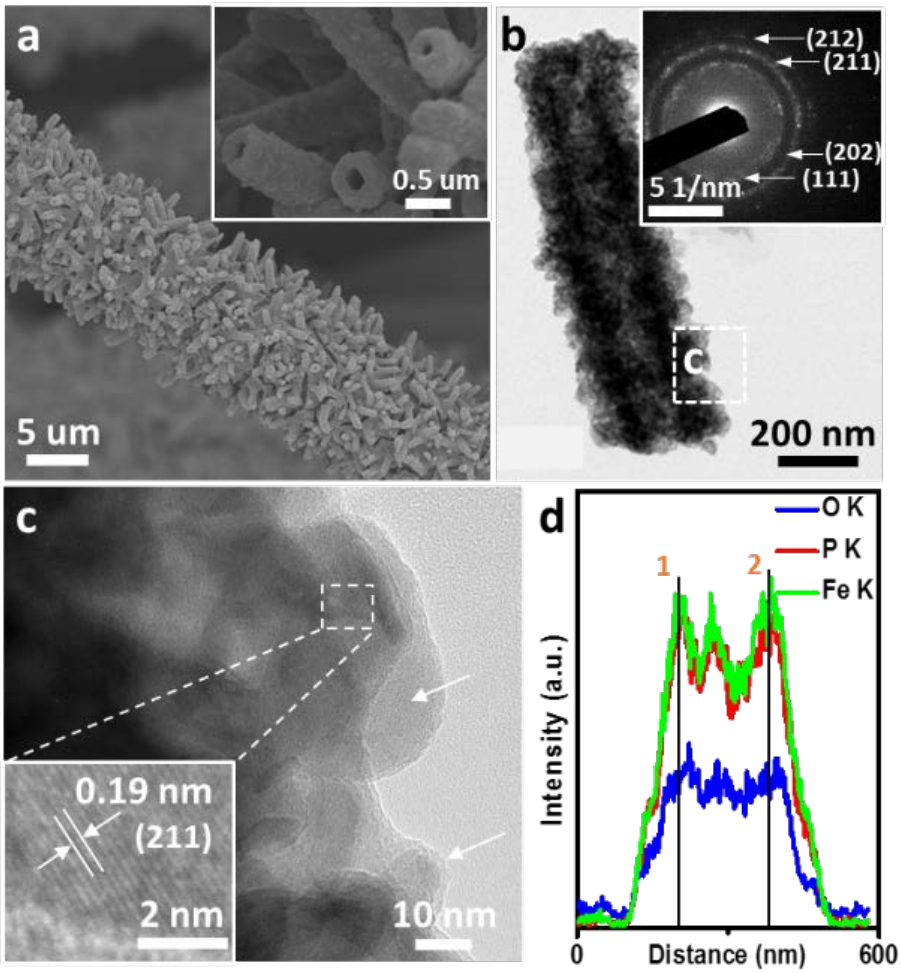

Figure 1. (a) SEM (inset: magnified SEM image); (b) TEM (inset: SAED pattern of IPNT) and (c) HRTEM image of IPNTs (inset: enlarged HRTEM image). (d) EDS line scan curves across the IPNT indicated by a line in (Figure S3a).

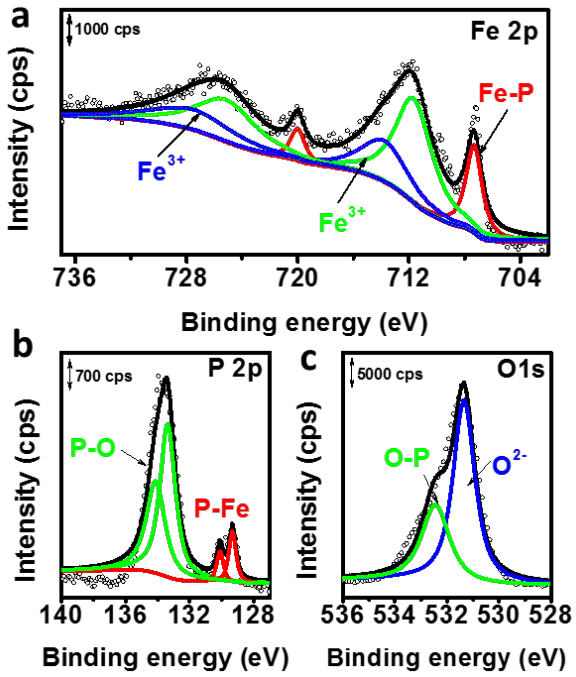

Figure 2. XPS spectra of Fe 2p (a), P 2p (b), and O 1s (c) for IPNTs.

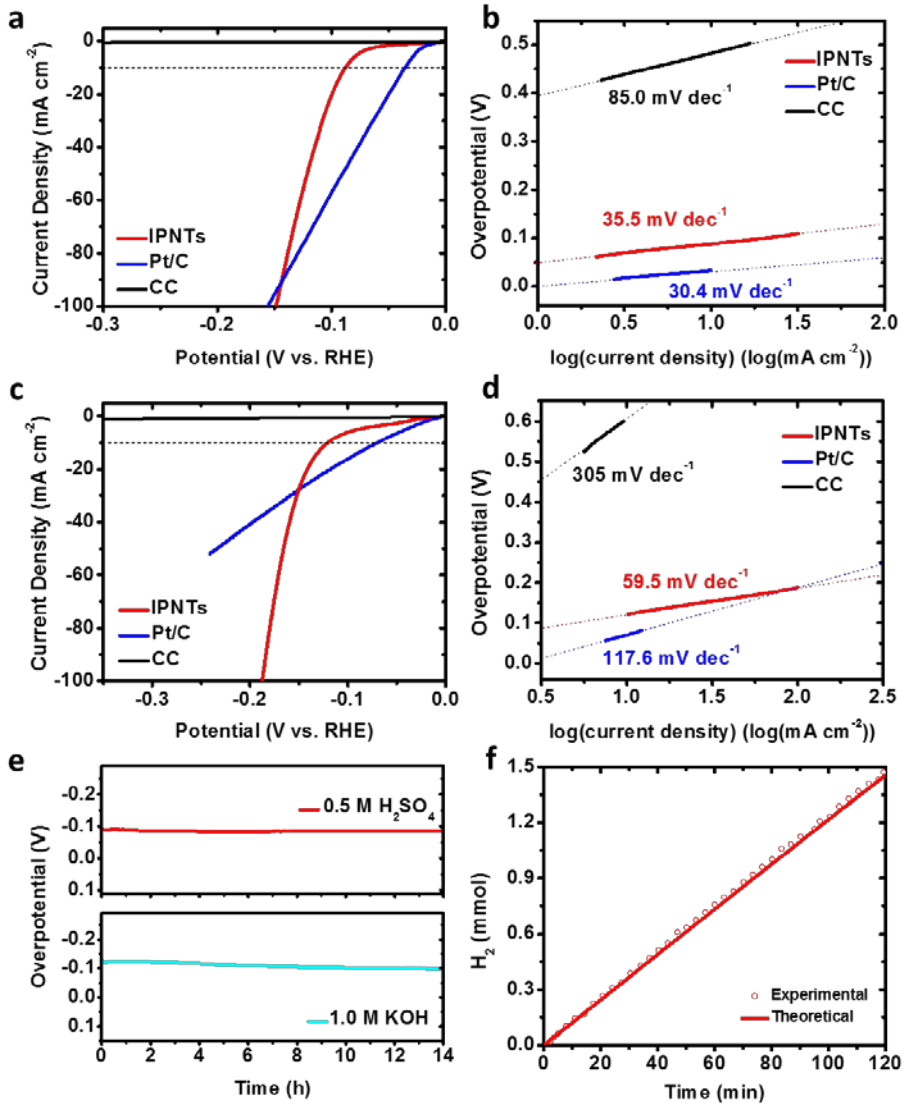

Figure 3. (a) *i*R-corrected LSV curves measured in 0.5 M H_2SO_4 and (b) corresponding Tafel slopes. (c) *i*R-corrected LSV curves measured in 1.0 M KOH and (d) corresponding Tafel slopes. (e) Durability test at -10 mA cm^{-2} in both acidic and basic electrolyte. (f) Faradic efficiency of the HER in 1.0 M KOH at η =216 mV.

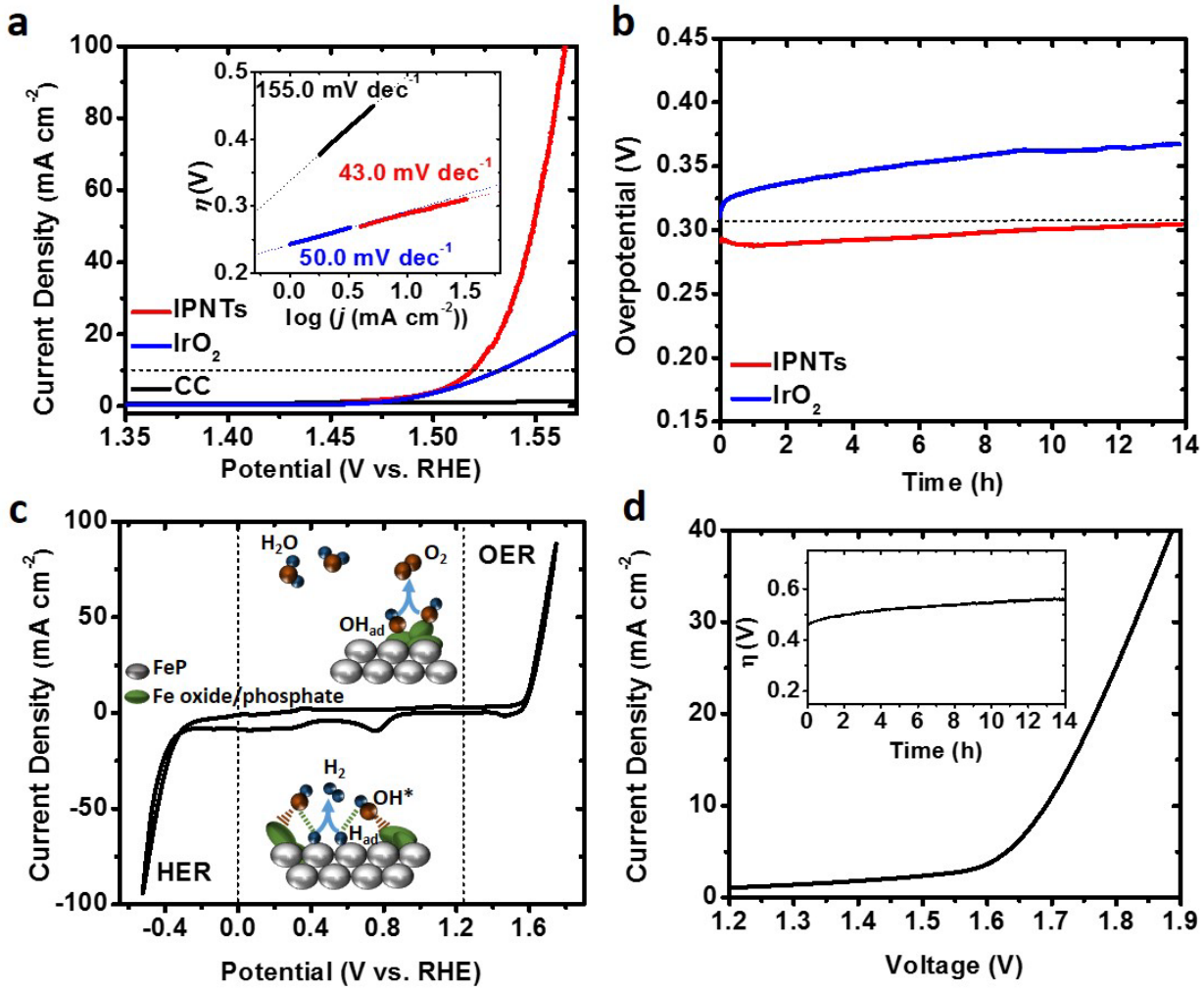

Figure 4. (a) *i*R-corrected LSV curves measured in 1.0 M KOH (inset: the corresponding Tafel slopes). (b) Durability test in 1.0 M KOH solution at 10 mA cm^{-2}. (c) CV curve of IPNTs in 1.0 M KOH with a scan rate of 50 mV s^{-1} (inset: proposed bi-functional mechanism of the catalyst for overall water splitting). (d) Current-potential response of a two-electrode alkaline electrolyzer (Inset: galvanostatic electrolysis in 1.0 M KOH at 10 mA cm^{-2} over 14 h).

TOC

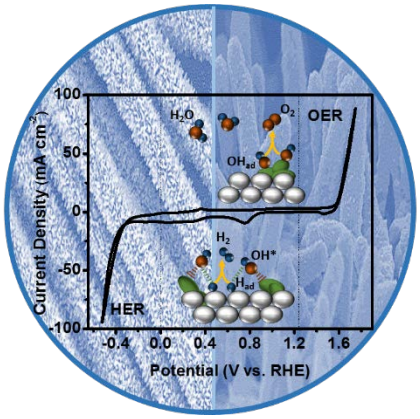

Bifunctional electrode for water splitting: Flexible electrode based on carbon cloth substrate and iron phosphide nanotube coated with an iron oxide/phosphate layer demonstrates the Janus electrocatalytic activity for overall water splitting. The surface iron oxide/phosphate formed *in-situ* is proposed to improve the HER activity by facilitating the water dissociation step and serves directly as the catalytically-active component for the OER process.